Terr. Atmos. Ocean. Sci., Vol. 31, No. 2, 211-225, April 2020 doi: 10.3319/TAO.2019.08.16.01

Effects of convection-SST interactions on the South China Sea summer monsoon onset in a multiscale modeling framework model

Kuan-Ting Kuo, Wei-Ting Chen *, and Chien-Ming Wu

Department of Atmospheric Sciences, National Taiwan University, Taipei City, Taiwan

Article history:

Received 30 March 2019
Revised 24 June 2019
Accepted 16 August 2019

Keywords:

Superparameterization, Slab ocean model, South China Sea Summer Monsoon

Citation:

Kuo, K.-T., W.-T. Chen, and C.-M. Wu, 2020: Effects of convection-SST interactions on the South China Sea summer monsoon onset in a multiscale modeling framework model. Terr. Atmos. Ocean. Sci., 31, 211-225, doi: 10.3319/TAO.2019.08.16.01

ABSTRACT

The present study explores the effects of convection-SST interactions on the onset of the South China Sea Summer Monsoon simulated by the superparameterized Community Atmosphere Model (SPCAM). The SPCAM is a global multi-scale modeling framework that embeds a 2-D cloud-resolving model in each grid column to replace the conventional convective parameterization. Two experiments are performed: CTRL uses prescribed sea surface temperature climatology, and CPL is coupled to a slab ocean model (SOM). The bias of excessive seasonal mean precipitation over Asia during boreal summer in CTRL is reduced in CPL. In the South China Sea, the seasonal evolution of precipitation and 850 hPa winds is more realistic in the coupled simulation. During the pre-onset stage, the mean pattern of synoptic flow and precipitation, as well as the land-ocean diurnal cycle contrast is also improved in CPL. The coupling to SOM does not change the sensitivity of precipitation to column moisture in the SPCAM. The improvements in CPL can be partly attributed to the lower SST in response to air-sea interactions, and also partly to the suppression of heavy precipitation under high SST regime likely associated with a different atmospheric meridional circulation. Our current results demonstrated that the SPCAM coupled with SOM could be a potential tool to study the interactions among convection, SST, and large-scale atmospheric circulation from seasonal to sub-seasonal time scales.

1. INTRODUCTION

Simulating the Asian monsoon is a great challenge to global climate models (GCMs). Previous studies have identified biases in the mean state precipitation and circulation of the Asian monsoon (e.g., Wang et al. 2005; Annamalai et al. 2007, 2017; Randall et al. 2007; Zhou et al. 2009, 2016; Cook et al. 2012; Kitoh et al. 2013; Sperber et al. 2013; Song and Zhou 2014a, b). The monsoon systems involve the regionally-distinct interactions between atmospheric circulation and rainfall (Webster et al. 1998; Sperber et al. 2013). Previous works have associated the biases in monsoon simulation to various components in the climate system, such as the atmosphere-ocean coupling (DeMott et al. 2007, 2011), convection parameterizations (Slingo et al. 1994; Rajendran et al. 2002; Mukhopadhyay et al. 2010; Bush et al. 2015), orographic blocking and heating (Boos and Hurley 2013; Wu and Hsu 2016; Wu et al. 2017, 2018), large-scale circulation (Sperber and Palmer 1996; Gadgil and Sajani 1998; Bollasina and Nigam 2009), land-sea thermal contrast (Zhou and Zou 2010), sea surface temperature (SST) pattern (Bollasina and Nigam 2009; Levine and Turner 2012; Levine et al. 2013; Marathayil et al. 2013), the interannual variability (Zhou et al. 2009; Song and Zhou 2014b; Li et al. 2015), and the underestimation of sub-seasonal (2 - 128 days) variabilities (Kang et al. 2002; Waliser et al. 2003; Lin et al. 2008).

The South China Sea (SCS) summer monsoon is a subsystem of the Asian monsoon (Ding et al. 2004), and connects the other three summer monsoon systems, namely, the South Asia, the East Asia (EA), and the western North Pacific (WNP) summer monsoons (Tao et al. 1987; Wang and Lin 2002). The unique feature of the SCS summer monsoon (SCSSM) is the sharp, abrupt reversal of low-level winds from northeasterly to southwesterly and rainfall burst during its onset period. This drastic phenomenon occurs climatologically around the 28th Julian Pentad in mid-May, but with significant interannual variation (Wang and Lin 2002;

* *Corresponding author*
E-mail: weitingc@ntu.edu.tw

Wang et al. 2009). The SCS summer monsoon is a challenging and yet important area for studying multi-scale interactions (Chang et al. 2006; Wang et al. 2009).

The SCS is surrounded by islands and continents with complex topography. Diurnal cycle is active over land surrounding the SCS from April (pre-onset) to Boreal summer (Aves and Johnson 2008; Li et al. 2010). The ocean precipitation becomes active sharply after onset and is dominated by organized coastal systems that are sensitive to vertical wind shear (Johnson et al. 2005; Xu and Rutledge 2018). Using the multi-year hindcast approach, Chen et al. (2019a) identified that the precipitation bias during the SCSSM onset period in a conventional GCM, the National Center of Atmospheric Research (NCAR) Community Atmospheric Model (CAM) version 5, is associated with the weaker diurnal cycle over land, the insufficient sensitivity of the cumulus parameterization to moisture, and the inappropriate representation of coastal organized convection.

On the other hand, previous studies using the Multiscale Modeling Framework (MMF) version of NCAR CAM version 3, the superparameterized CAM (SPCAM), have reported improvements, relative to the conventional CAM, in the simulated diurnal variation of rainfall (Khairoutdinov et al. 2005; Zhang et al. 2008; Pritchard and Somerville 2009), low-level moistening prior to major precipitation events (DeMott et al. 2007), and mean state of the Asian summer monsoon (DeMott et al. 2011). The MMF replaced the conventional cumulus parameterization in each grid column by a nested integration of a 2-dimensional (2D; x-z or y-z) cloud-resolving models (CRM) that explicitly simulates convection at the given grid-mean state variables (Khairoutdinov et al. 2005, 2008; DeMott et al. 2007). Cheng and Xu (2014) demonstrated that the organized mesoscale systems simulated in the SPCAM also exhibits strong sensitivity to the grid-scale vertical wind shear, and by varying the orientations of the CRM relative to the environmental wind shear can improve the simulated monsoon and large-scale circulation.

This study aims to investigate the effect of convection-SST interactions on the sharp transition of SCS summer monsoon onset simulated by the SPCAM. We will compare the SPCAM experiments with and without the coupling to a slab ocean model (SOM). Coupling to a SOM provides a method to study intraseasonal phenomena to seasonal transition (e.g., the Asian monsoon and the Madden-Julian oscillation) under a steady ocean mean state while allowing high frequency air-sea interactions. Here the convection-SST coupling refers to the process involving radiative balance in determining the fast SST variation (Grabowski 2006). When convection is strong, SST is cooled by stronger evaporation and reduced surface shortwave radiation. When subsidence dominates, enhanced surface shortwave heating leads to increasing SST. This fast interaction is especially prominent when the deep convection is explicitly simulated as in the superparameterized framework. With prescribed SST, such negative feedback is missing, which is the major reason of the biased boreal summer rainfall hotspots in the SPCAM simulations (Randall et al. 2016). Previous studies have shown that coupling SPCAM to a full ocean dynamic model improves the simulation of the Boreal Summer Intraseasonal Oscillation (BSISO) (DeMott et al. 2013, 2014) and Madden-Julian oscillation (MJO) (Kim et al. 2008; Benedict and Randall 2011; DeMott et al. 2014; Klingaman and Woolnough 2014; Stan 2018), due to strong convection-radiation-SST interactions, while the effects of convection-SST coupling on the sharp monsoon onset has not been examined before. Chen et al. (2019b) identified that the development of organized convection is the key of the moisture development over SCS and hence the SCSSM onset. In the SPCAM framework, the organized convection tends to be too strong and requires convection-SST coupling to reduce its variability; therefore, we expect by coupling to a SOM will lead to improvements in the sharp onset feature.

The manuscript is organized as follows. Section 2 describes the model and the experiment setup; The simulation results are presented in section 3. Discussions on the precipitation-moisture dependence and SST-precipitation-circulation relationships are provided in section 4. Section 5 gives a summary and conclusion.

2. MODEL AND DATA SET DESCRIPTION

2.1 Model Configuration and Experiment Design

The model used here is the superparameterized Community Earth System Model (SP-CESM), version 1.1.1, in which the atmospheric component uses the superparameterized Community Atmosphere Model (SPCAM). The SPCAM is run with CAM4 physics (Neale et al. 2010), and its horizontal resolution is 1.9° × 2.5° with 26 levels. The embedded CRM is the System for Atmospheric Modeling (SAM) using a single-moment five-species bulk microphysics scheme (Khairoutdinov and Randall 2003). It has 32 columns oriented in the north-south direction (y-z), with a horizontal resolution of 4 km and 24 vertical levels. The coupled slab ocean model (SOM) is taken from the CESM, which follows Bitz et al. (2012). It is constructed from the 20-year climatology of a fully coupled run. We note that the SOM configuration is more relevant for studying phenomenon at intraseasonal to seasonal time scales, but is not suitable for simulating interannual variability or climate changes because the ocean basic state is given through mixed-layer depths and oceanic mixed-layer heat fluxes.

We conduct two experiments in this study, and the only difference is the setting in the oceanic component. The first simulation (CTRL) uses a prescribed SST from default data for F2000 configuration in the CESM. This F2000 SST is monthly mean data constructed with present day climatology (1982 - 2001) and using linear-interpolation to each

model time steps. In the second simulation (CPL), the SOM coupled to the atmosphere. Both simulations are integrated for 10 years, and the hourly output fields are saved for analyses.

2.2 Observation and Reanalysis Data

The simulated results are compared with the following data sets during the year 1998 - 2014. Daily mean precipitation estimates are taken from the Tropical Rainfall Measuring Mission (TRMM) 3B42 version 7 data set (Kummerow et al. 2000; Huffman et al. 2010). It is the combined Microwave Imager (TMI) and Precipitation Radar (PR) rainfall product, with a horizontal resolution of 0.25° × 0.25°. Daily mean SST is taken from the NOAA Optimum Interpolation Sea Surface Temperature (OISST) version 2 (Reynolds et al. 2002). Winds fields are taken from the 6-hourly European Centre for Medium-Range Weather Forecasts Reanalysis Interim (ERA-Int) (Dee et al. 2011) reanalysis with a horizontal resolution of 0.75° × 0.75°. The diagnostics of precipitation dependence on column water vapor (section 4.1) use atmospheric temperature observation from the 6-hourly 2.5° × 2.5° NCEP-DOE Reanalysis 2 (Kanamitsu et al. 2002), and the column water vapor (CWV) and precipitation data from the 0.25° × 0.25° TRMM Microwave Imager (TMI) v7r1 (Wentz et al. 2015).

3. RESULTS

3.1 Boreal Summer Climatology and Intraseasonal Variability

The simulated precipitation and SST during the boreal warm season (May to September, MJJAS) is compared with the observations in Fig. 1. The observation data are spatially re-gridded to the same resolution as the GCM grid (1.9° × 2.5°). The main bias in the prescribed-SST simulation (CTRL) is in the Asian monsoon region. CTRL produces too much rainfall especially around the coasts of India and Indochina. On average, it is about 3 mm d^{-1} higher than observation in these areas. This bias is also shown by Stan et

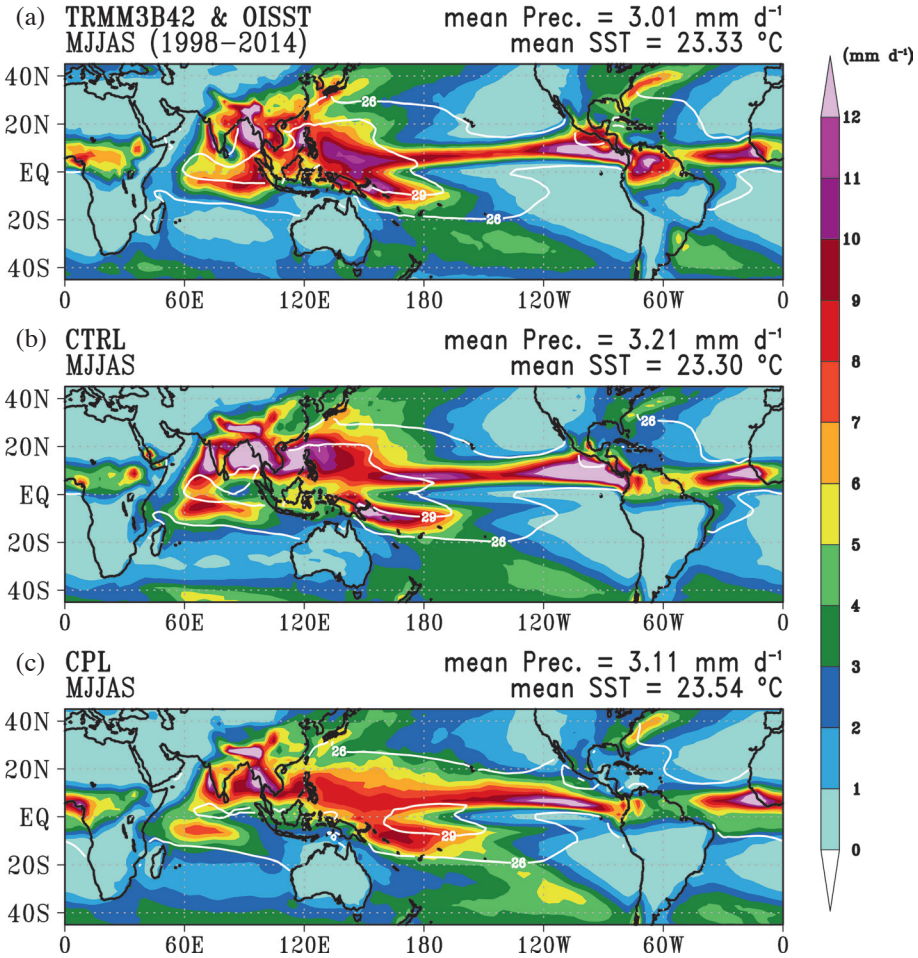

Fig. 1. The boreal summer (May to September) mean precipitation (color shading) and SST (contours at 26 and 29°C) from (a) TRMM 3B42 /OISST v2 (1998 - 2014) and the 10-year averages of (b) CTRL, and (c) CPL. The averaged values of precipitation and SST over 45°S - 45°N are shown on the upper-right of each panel. All observation data are regridded to the same resolution as the model output.

al. (2010) who simulate with a previous version of SPCAM. The main bias of the coupled simulation (CPL) is in the eastern Pacific caused by the Inter-Tropical Convergence Zone (ITCZ) shifting southward, while the precipitation bias is reduced around the Asian monsoon region and the Western Pacific. The MJJAS-mean SST in CPL is colder than observation over the western Pacific and the India Ocean, but it is higher over the eastern Pacific and the Southern Ocean. As a result, the global mean SST is slightly higher than the observation. In the Asian monsoon region, the SST in CPL is about 0.8 K colder than the observation.

Vertical structures of circulation also show different characteristics between the experiments. Figure 2 shows the MJJAS zonal mean meridional circulation over the Western Pacific. Reanalysis data and CPL show a double-cell pattern from 15°S to 30°N, while CTRL only shows a stronger cell in this region. This suggests that the meridional circulation in CTRL is too strong especially around the SCS monsoon region (5 - 20°N). CPL better represents the double-cell feature, although the circulation intensity is slightly weaker than that in the reanalysis.

Intraseasonal variability of precipitation is an essential feature for the Asian monsoon. Figure 3 shows the percentage of intraseasonal variance of 20-80-day bandpass filtered precipitation. Overall, the two experiments show similar magnitudes of intraseasonal precipitation percentage with the observation in the Asian monsoon region, but weaker intraseasonal precipitation is produced over the equatorial Indian Ocean comparing to the observation data. In the SCS, CPL has a higher ratio of intraseasonal precipitation than CTRL.

3.2 Monsoon Intensity and Seasonal Evolution

In this subsection, we take a close look at the general characteristics of the Asian monsoon. Figure 4 shows monsoon domain and monsoon intensity over Asia [following Wang and Ding (2008), Kim et al. (2011), and Wang et al. (2011); see figure caption for definition]. Over the land areas, both simulations show a stronger seasonal change in low-level winds but weaker monsoon intensity than observation/reanalysis. Over the ocean, the monsoon domain in CPL over West India, East Asia, and Western North Pacific (WNP) is closer to the observation than CTRL. In the SCS, CPL can simulate comparable monsoon intensity with observation, while CTRL produces very weak monsoon intensity.

Figure 5 shows seasonal evolutions of surface precipitation over the SCS region and U_{SCS} (averaged 850-hPa zonal wind over 5 - 15°N, 110 - 120°E, defined by Wang et al. 2004). The 30-day running mean (gray and blue lines) of precipitation in CTRL exhibits two monsoon-like periods in May to June and November to December, respectively, while the U_{SCS} evolution exhibits a single maximum around June. The unrealistic seasonal change and high total precipitation in winter lead to the weaker monsoon intensity as seen in Fig. 4. On the other hand, CPL exhibits one monsoon period as in the observation, with consistent sharp onset in both precipitation and U_{SCS}, although the onset timing is about one month later than the observed climatological onset at around mid-May.

3.3 Mean and Diurnal Cycle Precipitation over SCS During the Pre-Onset Stage

As a precursor of the East Asia summer monsoon, a reasonable simulation in the pre-onset stage of the SCS is important. Here we followed the definition of the SCS monsoon onset pentad proposed by Wang et al. (2004): (1) the U_{SCS} is larger than 0 (westerly wind), (2) there are at least 3 pentads of the U_{SCS} larger than 0 in following 4 pentads (including the onset pentad), and (3) the 4-pentad mean is larger than 1 m s^{-1}. The pre-onset stage in the present study is defined as 3 pentads before the onset pentad. Figure 6 shows the pre-onset composite mean precipitation and wind fields at 850 hPa. Observation shows a dry area over the SCS. CTRL produces too much rainfall over the ocean, leading to much smaller land-sea contrast of precipitation during the pre-onset stage. Therefore, the root mean square error (RMSE) is high, and the pattern correlation relative to the observation is low in CTRL. In CPL, although the dry area is displaced slightly northward, the pattern is much closer to the observation, including the land-sea contrast of precipitation and the synoptic-scale anticyclonic low-level flow over the SCS/WNP. The wind speed is too strong in both simulations, especially over Indochina to China, which is consistent with the overestimated seasonal wind change in Fig. 4.

Figure 7 shows the pre-onset composite diurnal range. The observed diurnal range of precipitation is low over the ocean but higher over land. This feature is not captured in CTRL, in which large diurnal range occurs over the SCS. This overestimation of ocean diurnal range is reduced in CPL, although over land there is still an underestimation in diurnal range compared to the observation, especially over the Philippines. This bias may be caused by the low resolution in our simulation to resolve the coastlines and the orographic effects. Figure 8 shows the pre-onset composite diurnal cycle of precipitation for land and ocean separately around the SCS region. The observation shows a maximum of precipitation around 17 LST and a minimum at 11 LST over the land area. In the ocean, the maximum occurs around noon, and the minimum occurs around midnight. The major difference between the two simulations is in the precipitation amount over the ocean: the overestimation in ocean precipitation is reduced in CPL through the day. Also, the maximum over the ocean in CTRL occurs too earlier (05 - 09 LST), while CPL exhibits peak time around (08 - 14 LST), which is closer to the observation. Over the land area, the two simulations are similar to each other. They

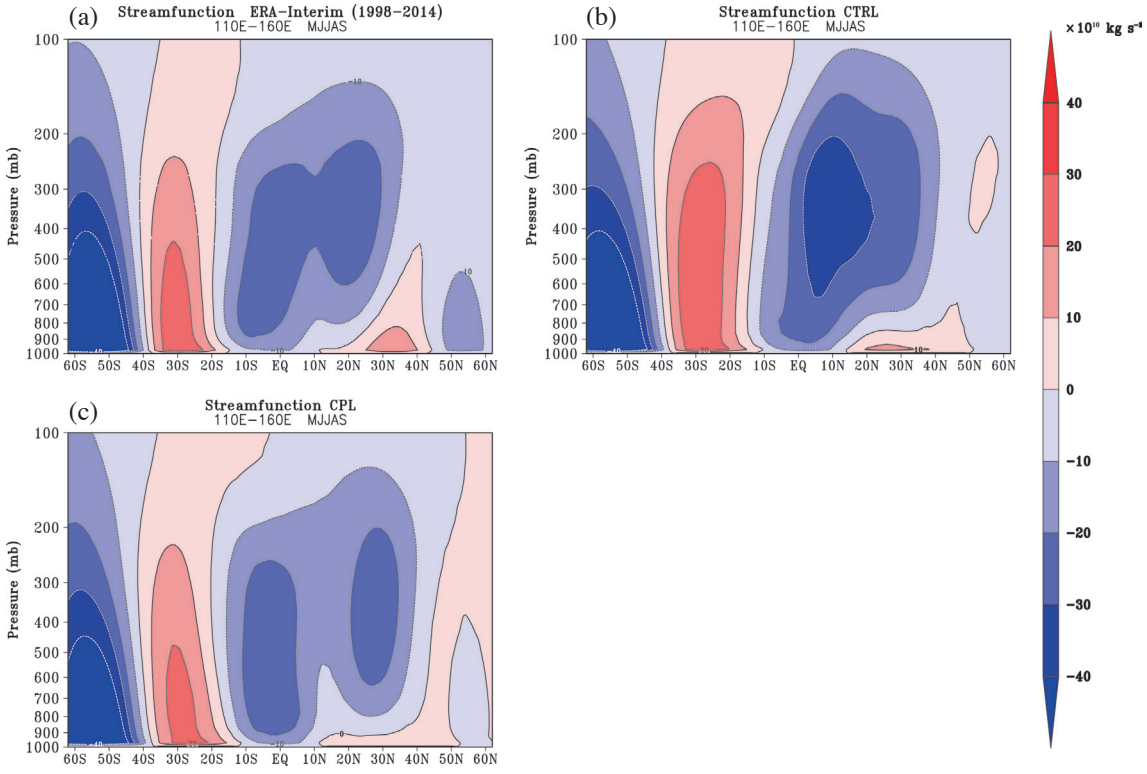

Fig. 2. Boreal summer (May - September) mean streamfunction (in 10^{10} kg s^{-1}) for zonal mean meridional circulation averaged between 110 and 160°E from (a) ERA-Int (1998 - 2014) and 10-year averages of (b) CTRL, and (c) CPL.

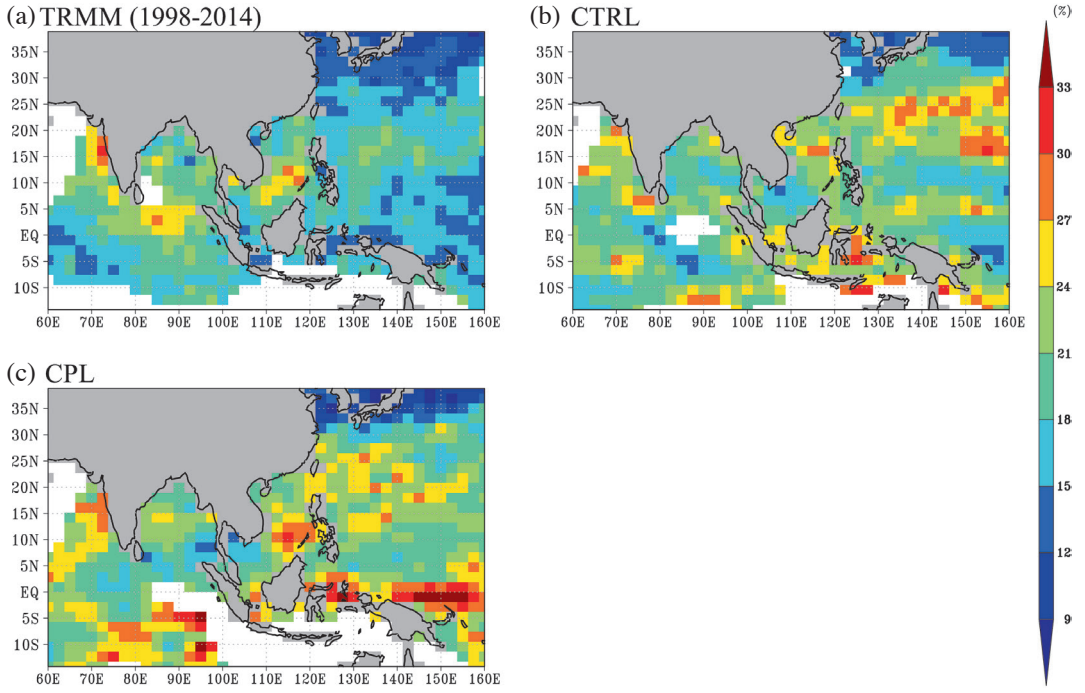

Fig. 3. The percentage of intraseasonal variance of precipitation over the ocean during the boreal summer (May to September) from (a) TRMM 3B42 (1998 - 2014, re-gridded to model resolution) and the 10-year simulations of (b) CTRL, and (c) CPL. The color shading shows the variance percentage of 20-80-day bandpass-filtered precipitation comparing to unfiltered variance. The grids with mean precipitation < 3 mm d^{-1} are masked in white. The land areas are colored gray.

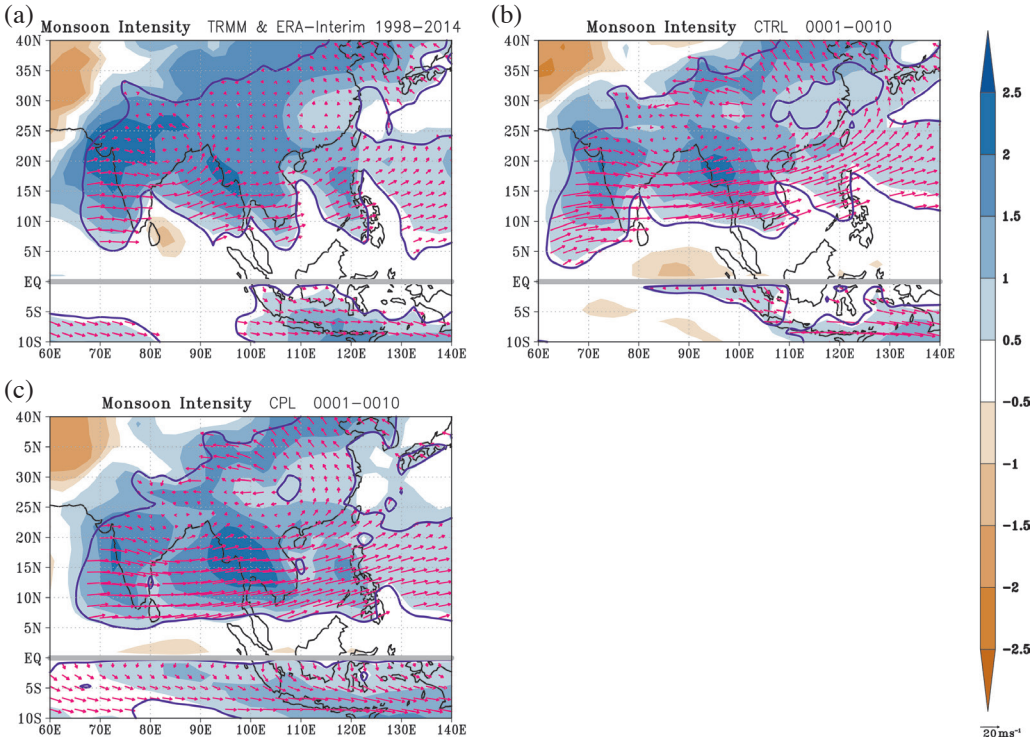

Fig. 4. Monsoon domain (enclosed by the blue contour), monsoon intensity (color shading), and seasonal change in 850 hPa winds (vectors) over Asia from (a) TRMM 3B42 precipitation/ERA-Int winds (1998 - 2014) and the 10-year averages of (b) CTRL, and (c) CPL. Following Wang and Ding (2008), Kim et al. (2011), and Wang et al. (2011), the monsoon domain represents the region where annual range of precipitation > 2.5 mm d^{-1}, and the monsoon intensity is the ratio of the annual range over the annual mean precipitation. The annual range of precipitation (as well as the seasonal change in wind fields) in the Northern Hemisphere is defined as boreal summer (May to September) mean minus the boreal winter (November to March) mean, and reversely over the Southern Hemisphere.

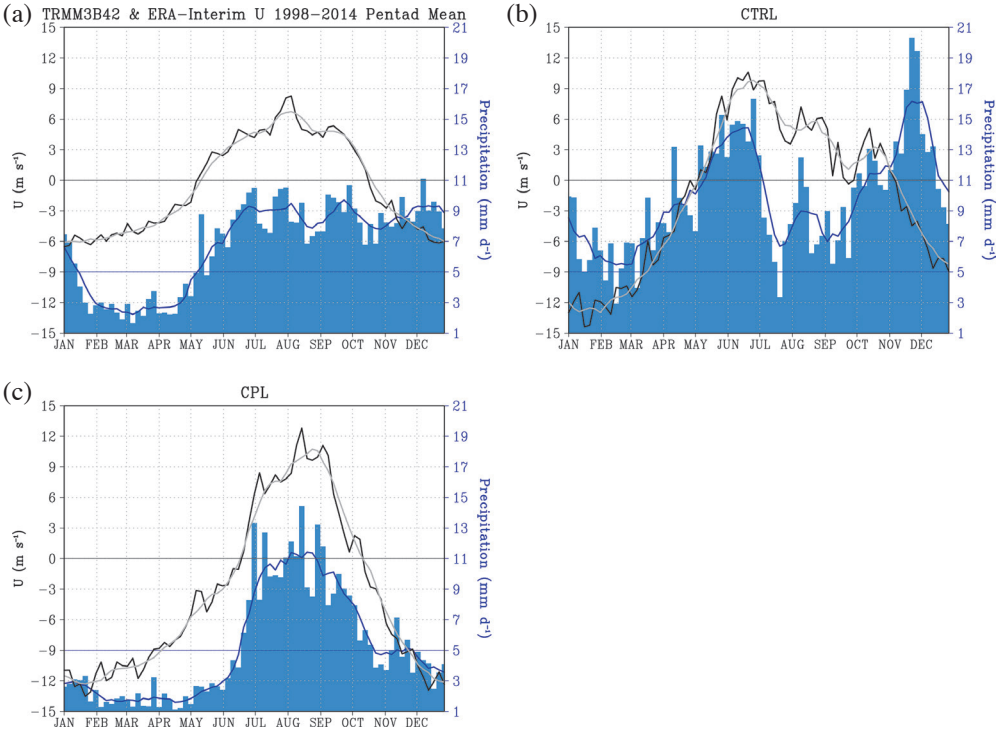

Fig. 5. Annual cycle of zonal wind and precipitation over the SCS (5 - 15°N, 110 - 120°E) from (a) TRMM 3B42 precipitation/ERA-Int winds (1998 - 2014) and the 10-year averages of (b) CTRL, and (c) CPL. The black (gray) line is pentad (30-day running) mean of zonal wind. The blue bar (line) is pentad (30-day running) mean of precipitation.

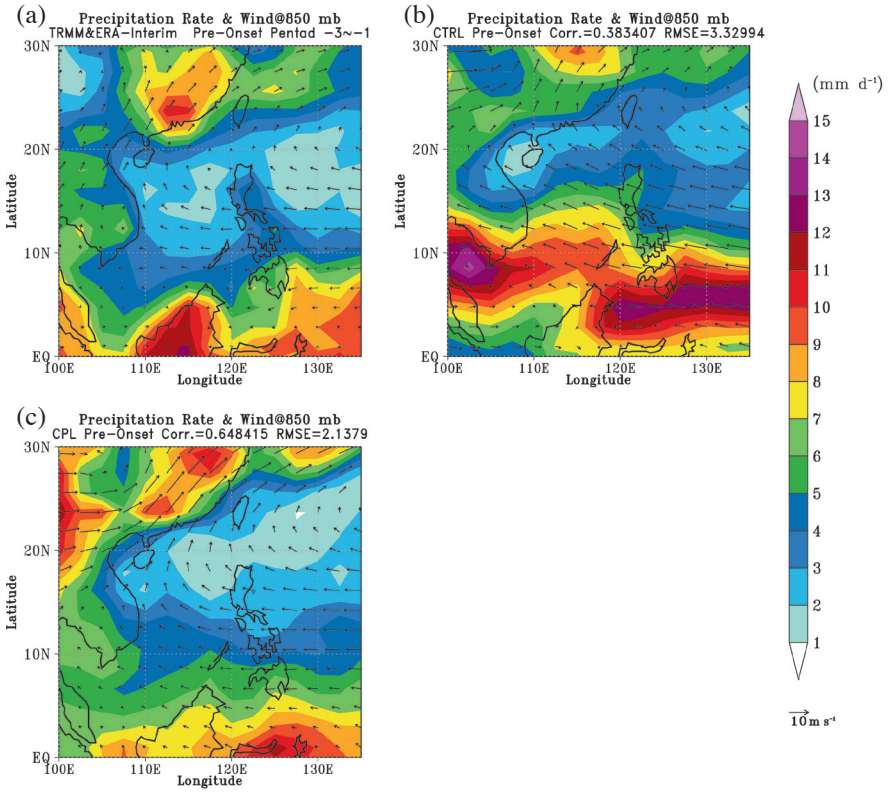

Fig. 6. The composite precipitation (color shading) and wind field at 850 hPa (vectors) averaged over the 3 pentads before the SCSSM onset from (a) TRMM 3B42 precipitation/ERA-Int winds (1998 - 2014, re-gridded to model resolution) and the 10-year averages of (b) CTRL, and (c) CPL. The definition of the SCS monsoon onset pentad proposed by Wang et al. (2004) (see text for more details). The pattern correlation and the RMSE of precipitation compared with TRMM 3B42 are shown at the top of (b) and (c).

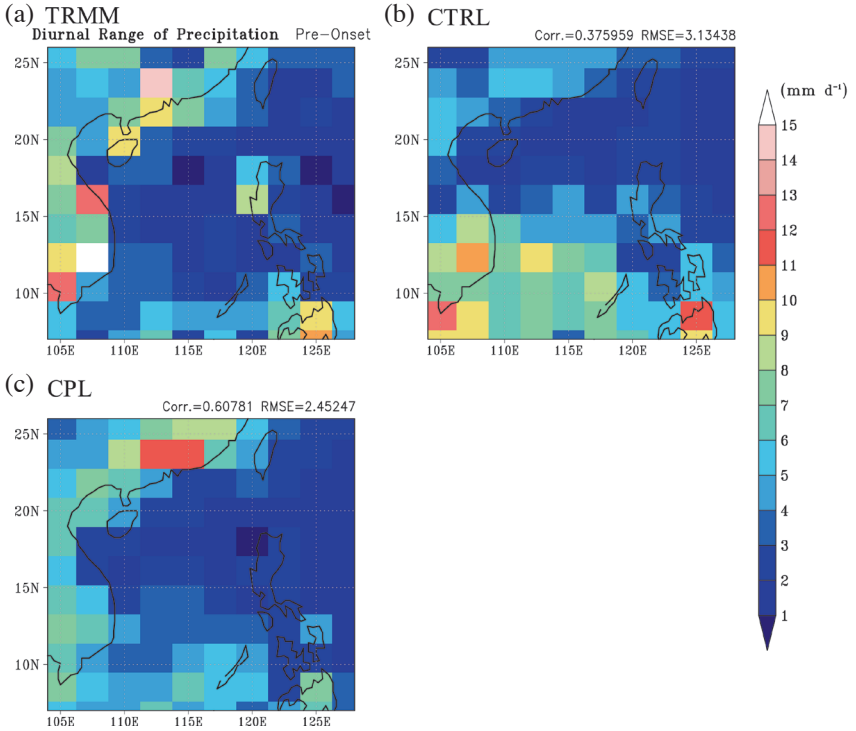

Fig. 7. The composite diurnal range of precipitation averaged over the 3 pentads before the SCSSM onset from (a) TRMM 3B42 (1998 - 2014, re-gridded to model resolution) and the 10-year averages of (b) CTRL, and (c) CPL. The pattern correlation and the RMSE compared with TRMM 3B42 are shown at the top of (b) and (c) (in mm day^{-1}).

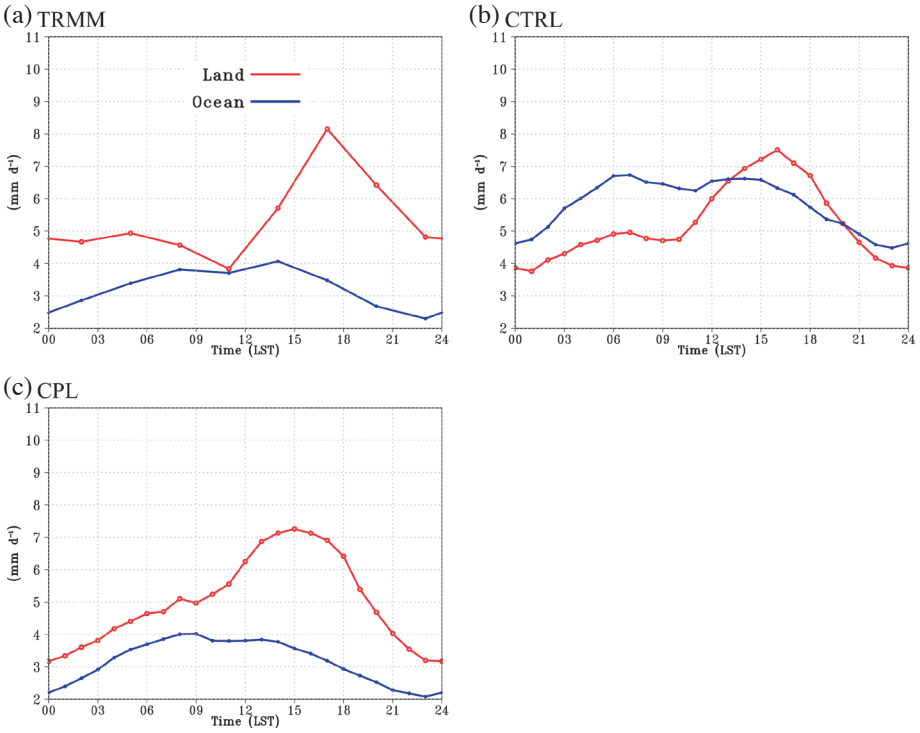

Fig. 8. The composite diurnal cycle over SCS (7 - 26°N, 104 - 128°E, the domain in Fig. 7) and averaged over the 3 pentads before the SCSSM onset from (a) TRMM 3B42 (1998 - 2014) and the 10-year averages of (b) CTRL, and (c) CPL. The red line is the average over land only, and the blue line is over ocean only. The local standard time (LST) is based on +8 UTC.

both underestimate the precipitation at midnight compared with the observation.

Based on the results in this section, the coupling to a SOM leads to the following improvements in the SPCAM simulation:

- Reducing the overestimation of boreal summer mean precipitation overestimation over Asia and western North Pacific, with a double-cell meridional circulation pattern closer to the reanalysis.
- More realistic monsoon domain and monsoon intensity over the ocean; better onset evolution over the SCS, with a circulation change consistent with the sharp precipitation increase.
- Stronger land-ocean contrast in mean and diurnal cycle precipitation during the SCS pre-onset period, with more accurate synoptic-scale horizontal circulation.

In the next section, we will investigate the differences between the two simulations from the perspectives of (1) sensitivity of precipitation to column moisture and (2) relationships between precipitation, SST, and large-scale circulation in the next section.

4. DISCUSSION

4.1 Dependence of Precipitation on Column Water Vapor

The diagnostics of Kuo et al. (2018) is used to identify the sensitivity of precipitation to ambient moisture over the tropical ocean, as shown in Fig. 9. Each colored line represents the conditional sampling by a different value of mass-weighted column-averaged temperature. The observation shows a sharp precipitation pickup with increasing CWV, and all the colored lines can be collapsed nicely when shifting CWV by the critical column water vapor (w_c). On the other hand, both simulations show a dependence of precipitation pickup on temperature (i.e., lines are spread out along CWV-w_c), and the slopes of the fitted pickup lines are flatter, indicating weaker precipitation efficiency, for the high-temperature condition. This leads to bias in the probability density function (PDF) of the simulated CWVs, which do not immediately drop off as in the observation when CWV > w_c. Such bias becomes severer as the temperature gets higher, especially for 275 K in CTRL. In general, the diagnostic results show similar sensitivity of precipitation to CWV in the two simulations.

4.2 The Relationship Between Precipitation, SST, and Circulation

In the coupled-SOM simulation, the SST is allowed to respond to atmosphere-ocean interactions. In Fig. 1, we found that the boreal summer global mean SST in CPL is only slightly higher than observation, but the regional SST over Asian monsoon domain the is colder. Part of the

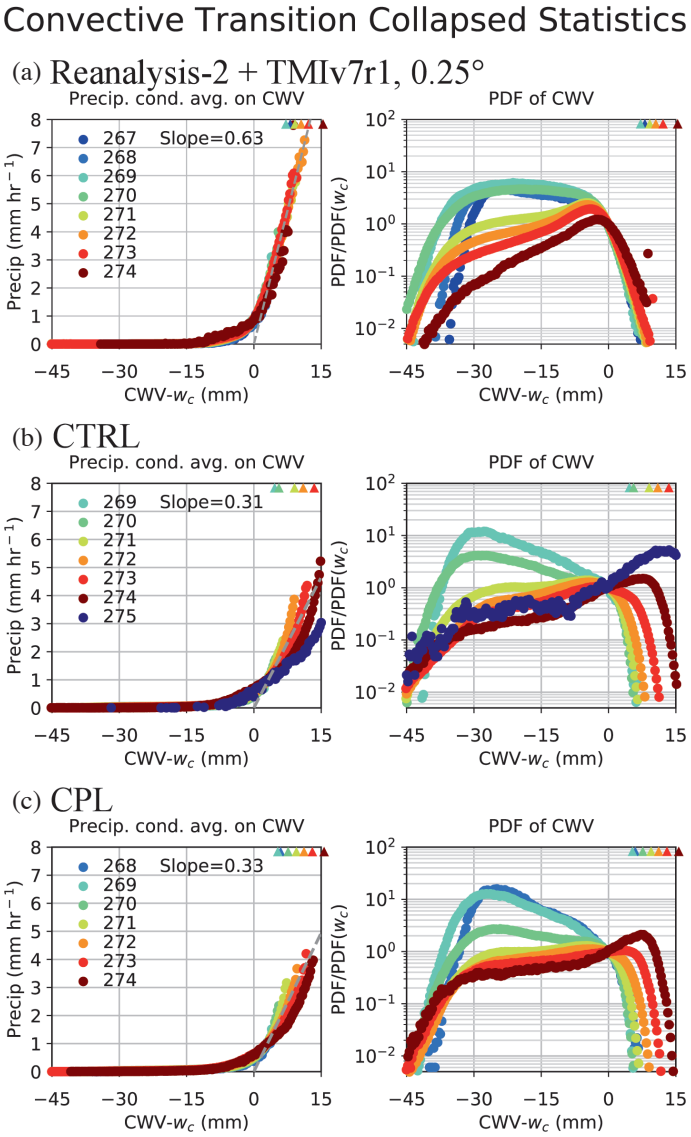

Fig. 9. Convective transition statistics for the ocean region 20°S - 20°N, 70 - 160°E and for (a) observation, (b) CTRL, and (c) CPL. The observation temperature is from the NCEP-DOE Reanalysis 2, and the column water vapor (CWV) and precipitation data are from TRMM Microwave Imager (TMI) v7r1. Different colors of dots represent the mass-weighted column average temperature from 267 to 275 K. The X axis is CWV relative to estimated critical column water vapor (w_c) which is the CWV when the average precipitation makes pickup. The left panel is conditional average precipitation on the relative CWV. The dashed line is the average precipitation pickup curve fitting. The right panel is probability density function (PDF) based on the relative CWV.

improvements in CPL identified in section 3 might be related to the lower SST over the Asian monsoon region. To understand the effects of lower SST, another experiment, named SST = SOM, is conducted. In this additional experiment, the SST is prescribed using the monthly mean SST saved during the 10-year integration of CPL. Most results of SST = SOM are similar to CPL, including the MJJAS mean precipitation, pre-onset precipitation, diurnal cycle of precipitation, and convective diagnostic result (e.g., Figs. 10a and b). Therefore, we can explain the improvements in these features in CPL (relative to CTRL) to the lower regional SST when it can interact with the atmosphere. However, the most apparent difference between CPL and SST = SOM is in the timing and transition of the SCSSM onset, as shown in Fig. 10c. The SCS monsoon onset date in SST = SOM is later than both CPL and CTRL, and the onset dates exhibit high interannual variability. This result implies that the dynamic interaction between the atmosphere and SST is required to capture the accurate timing of the sharp seasonal transition over the SCS. A similar situation may also occur in other regions with prominent sub-seasonal variability where convection-radiation-SST interactions are active.

The effects of the lower SST on precipitation in the

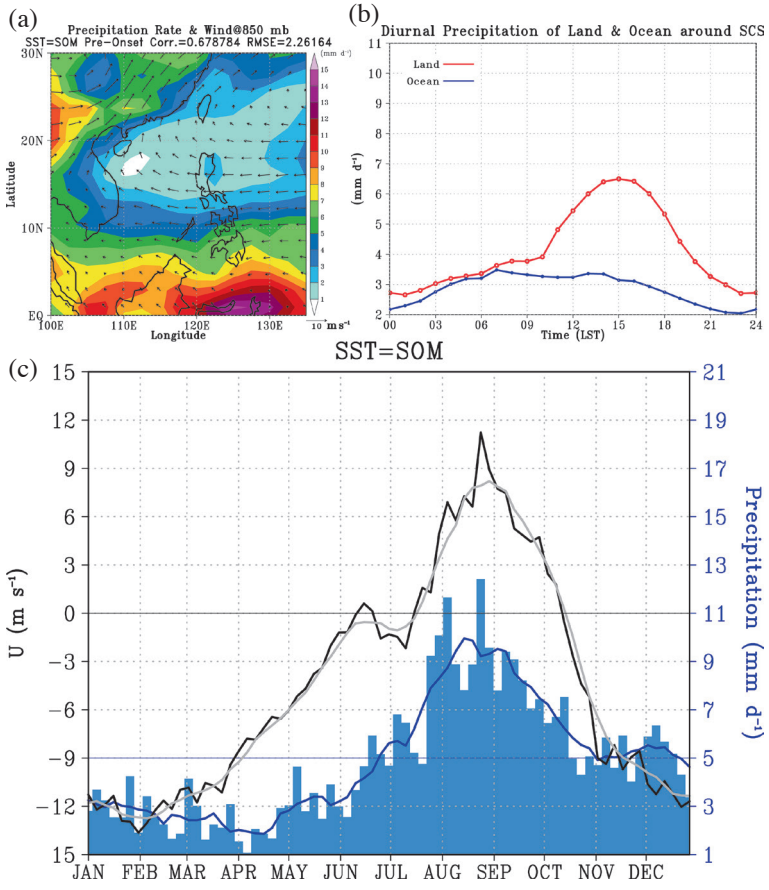

Fig. 10. As in (a) Fig. 6, (b) Fig. 8, and (c) Fig. 5 but for the experiment SST = SOM.

three simulations are illustrated by Fig. 11, which shows the precipitation intensity conditionally sampled by SST from each grid within the Asian monsoon region. For SSTs lower than 28°C, the observation and all experiments show that precipitation gradually increases with increasing SST, and the simulated precipitation intensity is close to the observation. For SSTs higher than 28°C, CTRL produces much stronger precipitation than observation, and keep increasing with higher SST. However, when the prescribed SST is also above 28°C in SST = SOM, the simulated precipitation intensity is much weaker and falls off with increasing SST, which is closer to the results in the observations and in CPL.

The atmospheric circulation may be one of the factors suppressing the precipitation over high SST regimes in SST = SOM. Figure 12 presents regions where the probability for heavy rainfall is low when high SST occurs (dotted areas). Such areas are broad in the observations (Fig. 12a) except over eastern Bay of Bengal, eastern tropical Indian Ocean, and Tropical Western Pacific. CPL captures most of these areas well with observation. SST = SOM shows a similar pattern with CPL. In CTRL, the areas of high SST but suppressed heavy precipitation is missing around 10 to 20°N. This is also the latitudinal band exhibiting significant bias in the meridional circulation over SCS/Western Pacific in CTRL (Fig. 2), indicating that the overestimation of precipitation in this area is likely associated with the bias in large-scale circulation under the prescribed climatological SST.

5. SUMMARY AND CONCLUSION

The present study investigated of effects of atmosphere-ocean interactions in a global MMF, the SPCAM, focusing on the features associated with the South China Sea Summer Monsoon Onset. In the 10-year simulation of SPCAM coupled to a slab ocean model, general improvements can be identified in boreal summer mean precipitation (Fig. 1) and meridional vertical circulation (Fig. 2), Asian monsoon domain over the ocean, and monsoon intensity over the SCS (Fig. 4), relative to the simulation with the F2000 SST. More specifically, the seasonal evolution of precipitation and winds over SCS is more realistic and clearer in the coupled simulation (Fig. 5), with more significant pre-onset suppression of ocean precipitation and diurnal cycle rainfall closer to the observations (Figs. 6, 7, and 8). The dependence of precipitation on column water vapor does not change significantly when coupled to the SOM (Fig. 9). The additional experiment using prescribed SST from the coupled simulation (SST = SOM) reveals that the colder SST can explain part of the

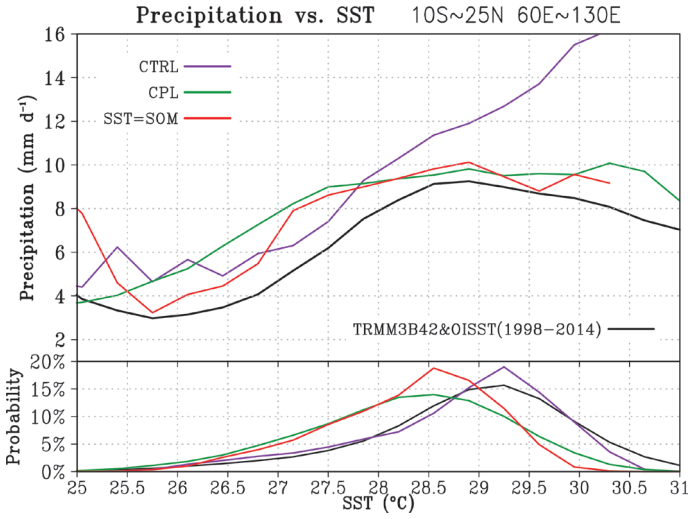

Fig. 11. Relationship between precipitation and SST for the region 10°S - 25°N, 60 - 130°E during the boreal summer (May to September). The observation of precipitation is from TRMM 3B42, and SST is from OISST v2 (1998 - 2014, re-gridded to model resolution). There are 20 bins of SST between 25 and 31°C. The upper penal shows the average precipitation rate over 0.08 mm d^{-1} in every bin of SST. The lower panel shows the occurrence probability of each SST bin.

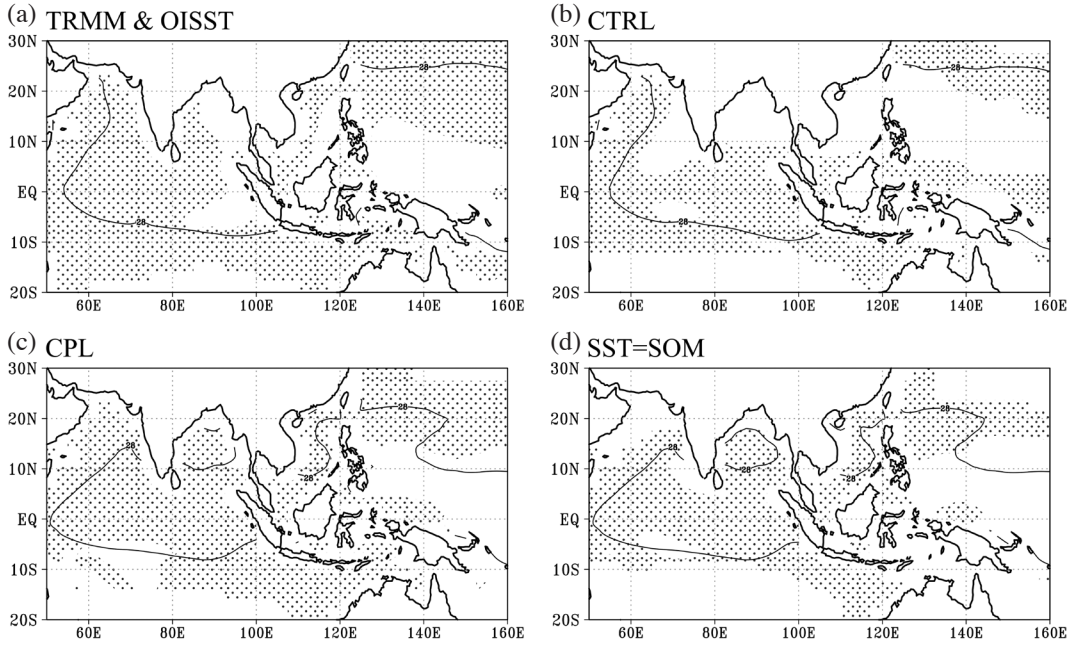

Fig. 12. The regions where the probability for heavy rainfall (10 mm d^{-1}) is lower than 20% when high SST regime (28°C) occurs during boreal summer (dotted area) for (a) observation, (b) CTRL, (c) CPL, and (d) SST = SOM. The contour line is boreal summer mean SST = 28°C.

improvements. Also, the precipitation-SST relationship in the coupled and SST = SOM simulations follows more closely to the observation, while the control simulation produces heavy precipitation too frequently over the high SST regime over SCS/Western Pacific (Figs. 11 and 12), which is likely associated to the bias in large-scale atmospheric circulation.

Although the SPCAM coupled with SOM exhibits bias in the precipitation-moisture dependence, our current results demonstrated that it is a useful tool to study the interactions among convection, SST, and large-scale atmospheric circulation from seasonal to sub-seasonal time scales, owing to the realistic representations of the sharp monsoon onset feature and the precipitation-SST-circulation relationship. This is an important foundation for subsequent study. In the future we will carry out more sensitivity studies to examine the details of how convection-related processes (e.g., wind gustiness, cloud radiation) and air-sea coupling frequency influence the coupling strength of the convection-SST feedback, and the sensitivity of the monsoon seasonal transition to the coupling strength.

Acknowledgements This work is supported by the Ministry of Science and Technology of Taiwan (MOST 106-2111-M-002-005, MOST 107-2119-M-002-024, MOST 107-2111-M-002-010-MY4). We sincerely thank Dr. Yi-Hung Kuo for providing the diagnostic package and discussion on the convection-moisture transition statistics. The datasets analyzed in the present study can be accessed through the following repositories: TRMM 3B42, https://pmm.nasa.gov/data-access/downloads/trmm (accessed 25 March 2019); NOAA OISST v2, http://www.esrl.noaa.gov/psd/data/gridded/data.noaa.oisst.v2.highres.html (accessed 25 March 2019); ERA-Int, http://apps.ecmwf.int/datasets/data/interim-full-daily/levtype=sfc/ (accessed 25 March 2019); NCEP-DOE Reanalysis 2, https://www.esrl.noaa.gov/psd/data/gridded/data.ncep.reanalysis2.html (accessed 25 March 2019); TMI v7r1, http://www.remss.com/missions/tmi/ (accessed 25 March 2019). The simulation outputs are available for online sharing upon request, due to the large volume of data sets and limited disk space.

REFERENCES

Annamalai, H., K. Hamilton, and K. R. Sperber, 2007: The South Asian Summer Monsoon and Its Relationship with ENSO in the IPCC AR4 Simulations. *J. Clim.*, **20**, 1071-1092, doi: 10.1175/JCLI4035.1. [Link]

Annamalai, H., B. Taguchi, J. P. McCreary, M. Nagura, and T. Miyama, 2017: Systematic Errors in South Asian Monsoon Simulation: Importance of Equatorial Indian Ocean Processes. *J. Clim.*, **30**, 8159-8178, doi: 10.1175/JCLI-D-16-0573.1. [Link]

Aves, S. and R. H. Johnson, 2008: The Diurnal Cycle of Convection over the Northern South China Sea. *J. Meteorol. Soc. Jpn.*, **86**, 919-934, doi: 10.2151/jmsj.86.919. [Link]

Benedict, J. J. and D. A. Randall, 2011: Impacts of idealized air-sea coupling on Madden-Julian oscillation structure in the superparameterized CAM. *J. Atmos. Sci.*, **68**, 1990-2008, doi: 10.1175/jas-d-11-04.1. [Link]

Bitz, C. M., K. M. Shell, P. R. Gent, D. A. Bailey, G. Danabasoglu, K. C. Armour, M. M. Holland, and J. T. Kiehl, 2012: Climate Sensitivity of the Community Climate System Model, Version 4. *J. Clim.*, **25**, 3053-3070, doi: 10.1175/JCLI-D-11-00290.1. [Link]

Bollasina, M. and S. Nigam, 2009: Indian Ocean SST, evaporation, and precipitation during the South Asian summer monsoon in IPCC-AR4 coupled simulations. *Climate Dyn.*, **33**, 1017-1032, doi: 10.1007/s00382-008-0477-4. [Link]

Boos, W. R. and J. V. Hurley, 2013: Thermodynamic Bias in the Multimodel Mean Boreal Summer Monsoon. *J. Clim.*, **26**, 2279-2287, doi: 10.1175/JCLI-D-12-00493.1. [Link]

Bush, S. J., A. G. Turner, S. J. Woolnough, G. M. Martin, and N. P. Klingaman, 2015: The effect of increased convective entrainment on Asian monsoon biases in the MetUM general circulation model. *Q. J. R. Meteorol. Soc.*, **141**, 311-326, doi: 10.1002/qj.2371. [Link]

Chang, C.-P., Z. Wang, and H. Hendon, 2006: The Asian Winter monsoon. In: Wang, B. (Ed.), The Asian Monsoon, Springer Praxis Books, Springer, Berlin, Heidelberg, 89-127, doi: 10.1007/3-540-37722-0_3. [Link]

Chen, W.-T., C.-M. Wu, and H.-Y. Ma, 2019a: Evaluating the bias of South China Sea summer monsoon precipitation associated with fast physical processes using a climate model hindcast approach. *J. Clim.*, **32**, 4491-4507, doi: 10.1175/JCLI-D-18-0660.1. [Link]

Chen, W.-T., C.-M. Wu, W.-M. Tsai, P.-J. Chen, and P.-Y. Chen, 2019b: Role of coastal convection to moisture buildup during the South China Sea summer monsoon onset. *J. Meteorol. Soc. Jpn.*, **97**, 1155-1171, doi: 10.2151/jmsj.2019-065. [Link]

Cheng, A. and K.-M. Xu, 2014: An explicit representation of vertical momentum transport in a multiscale modeling framework through its 2-D cloud-resolving model component. *J. Geophys. Res.*, **119**, 2356-2374, doi: 10.1002/2013JD021078. [Link]

Cook, K. H., G. A. Meehl, and J. M. Arblaster, 2012: Monsoon Regimes and Processes in CCSM4. Part II: African and American Monsoon Systems. *J. Clim.*, **25**, 2609-2621, doi: 10.1175/JCLI-D-11-00185.1. [Link]

Dee, D. P., S. M. Uppala, A. J. Simmons, P. Berrisford, P. Poli, S. Kobayashi, U. Andrae, M. A. Balmaseda, G. Balsamo, P. Bauer, P. Bechtold, A. C. M. Beljaars, L. van de Berg, J. Bidlot, N. Bormann, C. Delsol, R.

Dragani, M. Fuentes, A. J. Geer, L. Haimberger, S. B. Healy, H. Hersbach, E. V. Hólm, L. Isaksen, P. Kållberg, M. Köhler, M. Matricardi, A. P. McNally, B. M. Monge-Sanz, J.-J. Morcrette, B.-K. Park, C. Peubey, P. de Rosnay, C. Tavolato, J.-N. Thépaut, and F. Vitart, 2011: The ERA-Interim reanalysis: Configuration and performance of the data assimilation system. *Q. J. R. Meteorol. Soc.*, **137**, 553-597, doi: 10.1002/qj.828. [Link]

DeMott, C. A., D. A. Randall, and M. Khairoutdinov, 2007: Convective Precipitation Variability as a Tool for General Circulation Model Analysis. *J. Clim.*, **20**, 91-112, doi: 10.1175/JCLI3991.1. [Link]

DeMott, C. A., C. Stan, D. A. Randall, J. L. Kinter, and M. Khairoutdinov, 2011: The Asian Monsoon in the Superparameterized CCSM and Its Relationship to Tropical Wave Activity. *J. Clim.*, **24**, 5134-5156, doi: 10.1175/2011JCLI4202.1. [Link]

DeMott, C. A., C. Stan, and D. A. Randall, 2013: Northward Propagation Mechanisms of the Boreal Summer Intraseasonal Oscillation in the ERA-Interim and SP-CCSM. *J. Clim.*, **26**, 1973-1992, doi: 10.1175/JCLI-D-12-00191.1. [Link]

DeMott, C. A., C. Stan, D. A. Randall, and M. D. Branson, 2014: Intraseasonal Variability in Coupled GCMs: The Roles of Ocean Feedbacks and Model Physics. *J. Clim.*, **27**, 4970-4995, doi: 10.1175/JCLI-D-13-00760.1. [Link]

Ding, Y., C. Li, and Y. Liu, 2004: Overview of the South China sea monsoon experiment. *Adv. Atmos. Sci.*, **21**, 343-360, doi: 10.1007/BF02915563. [Link]

Gadgil, S. and S. Sajani, 1998: Monsoon precipitation in the AMIP runs. *Climate Dyn.*, **14**, 659-689, doi: 10.1007/s003820050248. [Link]

Grabowski, W. W., 2006: Impact of explicit atmosphere-ocean coupling on MJO-like coherent structures in idealized aquaplanet simulations. *J. Atmos. Sci.*, **63**, 2289-2306, doi: 10.1175/jas3740.1. [Link]

Huffman, G. J., R. F. Adler, D. T. Bolvin, and E. J. Nelkin, 2010: The TRMM Multi-Satellite Precipitation Analysis (TMPA). In: Gebremichael M. and F. Hossain (Eds.), Satellite Rainfall Applications for Surface Hydrology, Springer, Dordrecht, 3-22, doi: 10.1007/978-90-481-2915-7_1. [Link]

Johnson, R. H., S. L. Aves, P. E. Ciesielski, and T. D. Keenan, 2005: Organization of Oceanic Convection during the Onset of the 1998 East Asian Summer Monsoon. *Mon. Weather Rev.*, **133**, 131-148, doi: 10.1175/MWR-2843.1. [Link]

Kanamitsu, M., W. Ebisuzaki, J. Woollen, S.-K. Yang, J. J. Hnilo, M. Fiorino, and G. L. Potter, 2002: NCEP-DOE AMIP-II Reanalysis (R-2). *Bull. Amer. Meteorol. Soc.*, **83**, 1631-1644, doi: 10.1175/BAMS-83-11-1631. [Link]

Kang, I.-S., K. Jin, B. Wang, K.-M. Lau, J. Shukla, V. Krishnamurthy, S. Schubert, D. Wailser, W. Stern, A. Kitoh, G. Meehl, M. Kanamitsu, V. Galin, V. Satyan, C.-K. Park, and Y. Liu, 2002: Intercomparison of the climatological variations of Asian summer monsoon precipitation simulated by 10 GCMs. *Climate Dyn.*, **19**, 383-395, doi: 10.1007/s00382-002-0245-9. [Link]

Khairoutdinov, M. and D. A. Randall, 2003: Cloud Resolving Modeling of the ARM Summer 1997 IOP: Model Formulation, Results, Uncertainties, and Sensitivities. *J. Atmos. Sci.*, **60**, 607-625, doi: 10.1175/1520-0469(2003)060<0607:CRMOTA>2.0.CO;2. [Link]

Khairoutdinov, M., D. Randall, and C. DeMott, 2005: Simulations of the Atmospheric General Circulation Using a Cloud-Resolving Model as a Superparameterization of Physical Processes. *J. Atmos. Sci.*, **62**, 2136-2154, doi: 10.1175/JAS3453.1. [Link]

Khairoutdinov, M., C. DeMott, and D. Randall, 2008: Evaluation of the Simulated Interannual and Subseasonal Variability in an AMIP-Style Simulation Using the CSU Multiscale Modeling Framework. *J. Clim.*, **21**, 413-431, doi: 10.1175/2007JCLI1630.1. [Link]

Kim, H.-J., K. Takata, B. Wang, M. Watanabe, M. Kimoto, T. Yokohata, and T. Yasunari, 2011: Global Monsoon, El Niño, and Their Interannual Linkage Simulated by MIROC5 and the CMIP3 CGCMs. *J. Clim.*, **24**, 5604-5618, doi: 10.1175/2011JCLI4132.1. [Link]

Kim, H.-M., C. D. Hoyos, P. J. Webster, and I.-S. Kang, 2008: Sensitivity of MJO Simulation and Predictability to Sea Surface Temperature Variability. *J. Clim.*, **21**, 5304-5317, doi: 10.1175/2008JCLI2078.1. [Link]

Kitoh, A., H. Endo, K. Krishna Kumar, I. F. A. Cavalcanti, P. Goswami, and T. Zhou, 2013: Monsoons in a changing world: A regional perspective in a global context. *J. Geophys. Res.*, **118**, 3053-3065, doi: 10.1002/jgrd.50258. [Link]

Klingaman, N. P. and S. J. Woolnough, 2014: The role of air-sea coupling in the simulation of the Madden-Julian oscillation in the Hadley Centre model. *Q. J. R. Meteorol. Soc.*, **140**, 2272-2286, doi: 10.1002/qj.2295. [Link]

Kummerow, C., J. Simpson, O. Thiele, W. Barnes, A. T. Chang, E. Stocker, R. F. Adler, A. Hou, R. Kakar, F. Wentz, P. Ashcroft, T. Kozu, Y. Hong, K. Okamoto, T. Iguchi, H. Kuroiwa, E. Im, Z. Haddad, G. Huffman, B. Ferrier, W. S. Olson, E. Zipser, E. A. Smith, T. T. Wilheit, G. North, T. Krishnamurti, and K. Nakamura, 2000: The Status of the Tropical Rainfall Measuring Mission (TRMM) after Two Years in Orbit. *J. Appl. Meteorol.*, **39**, 1965-1982, doi: 10.1175/1520-0450(2001)040<1965:TSOTTR>2.0.CO;2. [Link]

Kuo, Y.-H., K. A. Schiro, and J. D. Neelin, 2018: Convective Transition Statistics over Tropical Oceans for Climate Model Diagnostics: Observational Baseline. *J. Atmos. Sci.*, **75**, 1553-1570, doi: 10.1175/JAS-D-17-0287.1. [Link]

Levine, R. C. and A. G. Turner, 2012: Dependence of Indian monsoon rainfall on moisture fluxes across the Arabian Sea and the impact of coupled model sea surface temperature biases. *Climate Dyn.*, **38**, 2167-2190, doi: 10.1007/s00382-011-1096-z. [Link]

Levine, R. C., A. G. Turner, D. Marathayil, and G. M. Martin, 2013: The role of northern Arabian Sea surface temperature biases in CMIP5 model simulations and future projections of Indian summer monsoon rainfall. *Climate Dyn.*, **41**, 155-172, doi: 10.1007/s00382-012-1656-x. [Link]

Li, G., S.-P. Xie, and Y. Du, 2015: Monsoon-Induced Biases of Climate Models over the Tropical Indian Ocean. *J. Clim.*, **28**, 3058-3072, doi: 10.1175/JCLI-D-14-00740.1. [Link]

Li, W., C. Luo, D. Wang, and T. Lei, 2010: Diurnal variations of precipitation over the South China Sea. *Meteorol. Atmos. Phys.*, **109**, 33-46, doi: 10.1007/s00703-010-0094-8. [Link]

Lin, J.-L., K. M. Weickman, G. N. Kiladis, B. E. Mapes, S. D. Schubert, M. J. Suarez, J. T. Bacmeister, and M.-I. Lee, 2008: Subseasonal Variability Associated with Asian Summer Monsoon Simulated by 14 IPCC AR4 Coupled GCMs. *J. Clim.*, **21**, 4541-4567, doi: 10.1175/2008JCLI1816.1. [Link]

Marathayil, D., A. G. Turner, L. C. Shaffrey, and R. C. Levine, 2013: Systematic winter sea-surface temperature biases in the northern Arabian Sea in HiGEM and the CMIP3 models. *Environ. Res. Lett.*, **8**, 014028, doi: 10.1088/1748-9326/8/1/014028. [Link]

Mukhopadhyay, P., S. Taraphdar, B. N. Goswami, and K. Krishnakumar, 2010: Indian Summer Monsoon Precipitation Climatology in a High-Resolution Regional Climate Model: Impacts of Convective Parameterization on Systematic Biases. *Weather Forecast.*, **25**, 369-387, doi: 10.1175/2009WAF2222320.1. [Link]

Neale, R. B., J. H. Richter, A. J. Conley, S. Park, P. H. Lauritzen, A. Gettelman, D. L. Williamson, P. J. Rasch, S. J. Vavrus, M. A. Taylor, W. D. Collins, M. Zhang, and S.-J. Lin, 2010: Description of the NCAR Community Atmosphere Model (CAM 4.0), NCAR Technical Note, NCAR/TN-485+STR, 212 pp.

Pritchard, M. S. and R. C. J. Somerville, 2009: Assessing the Diurnal Cycle of Precipitation in a Multi-Scale Climate Model. *J. Adv. Model. Earth Syst.*, **2**, doi: 10.3894/JAMES.2009.1.12. [Link]

Rajendran, K., R. S. Nanjundiah, and J. Srinivasan, 2002: Comparison of seasonal and intraseasonal variation of tropical climate in NCAR CCM2 GCM with two different cumulus schemes. *Meteorol. Atmos. Phys.*, **79**, 57-86, doi: 10.1007/s703-002-8229-0. [Link]

Randall, D. A., R. A. Wood, S. Bony, R. Colman, T. Fichefet, J. Fyfe, V. Kattsov, A. Pitman, J. Shukla, J. Srinivasan, R. J. Stouffer, A. Sumi, and K. E. Taylor, 2007: Climate Models and Their Evaluation. In: Solomon, S., D. Qin, M. Manning, Z. Chen, M. Marquis, K. B. Averyt, M. Tignor, and H. L. Miller (Eds.), Climate Change 2007: The Physical Science Basis, Contribution of Working Group I to the Fourth Assessment Report of the Intergovernmental Panel on Climate Change, Cambridge University Press, Cambridge, United Kingdom and New York, NY, USA.

Randall, D., C. DeMott, C. Stan, M. Khairoutdinov, J. Benedict, R. McCrary, K. Thayer-Calder, and M. Branson, 2016: Simulations of the tropical general circulation with a multiscale global model. *Meteorol. Monogr.*, **56**, 15.1-15.15, doi: 10.1175/amsmonographs-d-15-0016.1. [Link]

Reynolds, R. W., N. A. Rayner, T. M. Smith, D. C. Stokes, and W. Wang, 2002: An Improved In Situ and Satellite SST Analysis for Climate. *J. Clim.*, **15**, 1609-1625, doi: 10.1175/1520-0442(2002)015<1609:AIISAS>2.0.CO;2. [Link]

Slingo, J., M. Blackburn, A. Betts, R. Brugge, K. Hodges, B. Hoskins, M. Miller, L. Steenman-Clark, and J. Thuburn, 1994: Mean climate and transience in the tropics of the UGAMP GCM: Sensitivity to convective parametrization. *Q. J. R. Meteorol. Soc.*, **120**, 881-922, doi: 10.1002/qj.49712051807. [Link]

Song, F. and T. Zhou, 2014a: Interannual Variability of East Asian Summer Monsoon Simulated by CMIP3 and CMIP5 AGCMs: Skill Dependence on Indian Ocean-Western Pacific Anticyclone Teleconnection. *J. Clim.*, **27**, 1679-1697, doi: 10.1175/JCLI-D-13-00248.1. [Link]

Song, F. and T. Zhou, 2014b: The Climatology and Interannual Variability of East Asian Summer Monsoon in CMIP5 Coupled Models: Does Air-Sea Coupling Improve the Simulations? *J. Clim.*, **27**, 8761-8777, doi: 10.1175/JCLI-D-14-00396.1. [Link]

Sperber, K. R. and T. N. Palmer, 1996: Interannual Tropical Rainfall Variability in General Circulation Model Simulations Associated with the Atmospheric Model Intercomparison Project. *J. Clim.*, **9**, 2727-2750, doi: 10.1175/1520-0442(1996)009<2727:ITRVIG>2.0.CO;2. [Link]

Sperber, K. R., H. Annamalai, I.-S. Kang, A. Kitoh, A. Moise, A. Turner, B. Wang, and T. Zhou, 2013: The Asian summer monsoon: An intercomparison of CMIP5 vs. CMIP3 simulations of the late 20th century. *Climate Dyn.*, **41**, 2711-2744, doi: 10.1007/s00382-012-1607-6. [Link]

Stan, C., 2018: The role of SST variability in the simulation

of the MJO. *Climate Dyn*., **51**, 2943-2964, doi: 10.1007/s00382-017-4058-2. [Link]

Stan, C., M. Khairoutdinov, C. A. DeMott, V. Krishnamurthy, D. M. Straus, D. A. Randall, J. L. Kinter, and J. Shukla, 2010: An ocean-atmosphere climate simulation with an embedded cloud resolving model. *Geophys. Res. Lett*., **37**, doi: 10.1029/2009GL040822. [Link]

Tao, S. Y., L.-X. Chen, C.-P. Chang, and T. N. Krishnamurti, 1987: A review of recent research on the East Asian summer monsoon in China. Monsoon Meteorology, Oxford University Press, 60-92.

Waliser, D. E., K. Jin, I.-S. Kang, W. F. Stern, S. D. Schubert, M. L. C. Wu, K.-M. Lau, M.-I. Lee, V. Krishnamurthy, A. Kitoh, G. A. Meehl, V. Y. Galin, V. Satyan, S. K. Mandke, G. Wu, Y. Liu, and C.-K. Park, 2003: AGCM simulations of intraseasonal variability associated with the Asian summer monsoon. *Climate Dyn*., **21**, 423-446, doi: 10.1007/s00382-003-0337-1. [Link]

Wang, B. and H. Lin, 2002: Rainy Season of the Asian-Pacific Summer Monsoon. *J. Clim*., **15**, 386-398, doi: 10.1175/1520-0442(2002)015<0386:RSOTAP>2.0.CO;2. [Link]

Wang, B. and Q. Ding, 2008: Global monsoon: Dominant mode of annual variation in the tropics. *Dyn. Atmos. Oceans*, **44**, 165-183, doi: 10.1016/j.dynatmoce.2007.05.002. [Link]

Wang, B., H. Lin, Y. Zhang, and M.-M. Lu, 2004: Definition of South China Sea Monsoon Onset and Commencement of the East Asia Summer Monsoon. *J. Clim*., **17**, 699-710, doi: 10.1175/2932.1. [Link]

Wang, B., Q. Ding, X. Fu, I.-S. Kang, K. Jin, J. Shukla, and F. Doblas-Reyes, 2005: Fundamental challenge in simulation and prediction of summer monsoon rainfall. *Geophys. Res. Lett*., **32**, L15711, doi: 10.1029/2005GL022734. [Link]

Wang, B., F. Huang, Z. Wu, J. Yang, X. Fu, and K. Kikuchi, 2009: Multi-scale climate variability of the South China Sea monsoon: A review. *Dyn. Atmos. Oceans*, **47**, 15-37, doi: 10.1016/j.dynatmoce.2008.09.004. [Link]

Wang, B., H.-J. Kim, K. Kikuchi, and A. Kitoh, 2011: Diagnostic metrics for evaluation of annual and diurnal cycles. *Climate Dyn*., **37**, 941-955, doi: 10.1007/s00382-010-0877-0. [Link]

Webster, P. J., V. O. Magaña, T. N. Palmer, J. Shukla, R. A. Tomas, M. Yanai, and T. Yasunari, 1998: Monsoons: Processes, predictability, and the prospects for prediction. *J. Geophys. Res*., **103**, 14451-14510, doi: 10.1029/97JC02719. [Link]

Wentz, F. J., C. Gentemann, and K. A. Hilburn, 2015: Remote Sensing Systems TRMM TMI Daily Environmental Suite on 0.25 deg grid, version 7.1. Remote Sensing Systems. Available at http://www.remss.com/missions/tmi.

Wu, C.-H. and H.-H. Hsu, 2016: Role of the Indochina Peninsula Narrow Mountains in Modulating the East Asian–Western North Pacific Summer Monsoon. *J. Clim*., **29**, 4445-4459, doi: 10.1175/JCLI-D-15-0594.1. [Link]

Wu, C.-H., N. Freychet, C.-A. Chen, and H.-H. Hsu, 2017: East Asian presummer precipitation in the CMIP5 at high versus low horizontal resolution. *Int. J. Climatol*., **37**, 4158-4170, doi: 10.1002/joc.5055. [Link]

Wu, C.-H., M.-D. Chou, and Y.-H. Fong, 2018: Impact of the Himalayas on the Meiyu-Baiu migration. *Climate Dyn*., **50**, 1307-1319, doi: 10.1007/s00382-017-3686-x. [Link]

Xu, W. and S. A. Rutledge, 2018: Convective Variability Associated with the Boreal Summer Intraseasonal Oscillation in the South China Sea Region. *J. Clim*., **31**, 7363-7383, doi: 10.1175/JCLI-D-18-0091.1. [Link]

Zhang, Y., S. A. Klein, C. Liu, B. Tian, R. T. Marchand, J. M. Haynes, R. B. McCoy, Y. Zhang, and T. P. Ackerman, 2008: On the diurnal cycle of deep convection, high-level cloud, and upper troposphere water vapor in the Multiscale Modeling Framework. *J. Geophys. Res*., **113**, D16105, doi: 10.1029/2008JD009905. [Link]

Zhou, T. and L. Zou, 2010: Understanding the Predictability of East Asian Summer Monsoon from the Reproduction of Land-Sea Thermal Contrast Change in AMIP-Type Simulation. *J. Clim*., **23**, 6009-6026, doi: 10.1175/2010JCLI3546.1. [Link]

Zhou, T., B. Wu, and B. Wang, 2009: How Well Do Atmospheric General Circulation Models Capture the Leading Modes of the Interannual Variability of the Asian-Australian Monsoon? *J. Clim*., **22**, 1159-1173, doi: 10.1175/2008JCLI2245.1. [Link]

Zhou, T., A. G. Turner, J. L. Kinter, B. Wang, Y. Qian, X. Chen, B. Wu, B. Wang, B. Liu, L. Zou, and B. He, 2016: GMMIP (v1.0) contribution to CMIP6: Global Monsoons Model Inter-comparison Project. *Geosci. Model Dev*., **9**, 3589-3604, doi: 10.5194/gmd-9-3589-2016. [Link]